ORIGINAL RESEARCH—BASIC

Activated CD27$^+$PD-1$^+$ CD8 T Cells and CD4 T Regulatory Cells Dominate the Tumor Microenvironment in Refractory Celiac Disease Type II

Tessa Dieckman,[1,2] Mette Schreurs,[1] Ciska Lindelauf,[1] Ahmed Mahfouz,[3,4] Caroline R. Meijer,[5] Louise Pigeaud,[5] Vincent van Unen,[1] Gerd Bouma,[2] and Frits Koning[1]

[1]Department of Immunology, Leiden University Medical Center, Leiden, the Netherlands; [2]Department of Gastroenterology and Hepatology, Amsterdam UMC, Vrije Universiteit Amsterdam, Amsterdam Gastroenterology Endocrinology Metabolism, Amsterdam, the Netherlands; [3]Delft Bioinformatics Lab, Delft University of Technology, Delft, the Netherlands; [4]Department of Human Genetics, Leiden University Medical Center, Leiden, the Netherlands; and [5]Department of Paediatrics, Willem Alexander Children's Hospital, Leiden University Medical Center, Leiden, the Netherlands

BACKGROUND AND AIMS: Refractory celiac disease type II (RCDII) is characterized by a clonally expanded aberrant cell population in the small intestine. The role of other tissue-resident immune subsets in RCDII is unknown. Here, we characterized CD8 and CD4 T cells in RCDII duodenum at the single-cell level and *in situ*. **METHODS:** We applied mass cytometry on CD45$^+$ duodenal cells derived from intestinal biopsies (n = 23) and blood samples (n = 20) from RCDII patients and controls. Additionally, we analyzed intestinal biopsies from celiac disease (n = 11) and RCDI (n = 2) patients. We performed single-cell RNA-sequencing on CD45$^+$ duodenal cells derived from a RCDII patient, immunofluorescence staining for *in situ* analysis and flow cytometry for phenotyping of RCDII aberrant and CD8 T cells. **RESULTS:** Compared to healthy controls, we observed that CD27$^+$PD-1$^+$ memory CD8$\alpha\beta$ cells and CD4 T regulatories (Tregs) were more abundant in RCDII duodenum (CD8 **0.0029; CD4 ***0.0001). The CD27$^+$PD-1$^+$ memory CD8$\alpha\beta$ cells expressed the tissue-resident marker CD69, immunoregulatory markers (*TIGIT, HAVCR2, TNFRSF9)*, NKG2A, were enriched for activated pathways and displayed cytotoxic gene signatures (*NKG7, PRF1, GZMA)*. The absence of CD103 accords with their localization in the lamina propria as determined by *in situ* analysis. The CD25$^+$FoxP3$^+$CD27$^+$CD127$^{dim/-}$ CD4 Tregs expressed *IL1R2* and *IL32* and costimulatory molecules (*TNFSRS4*, *ICOS* and *TNFRSF18*) and resided in the lamina propria as well. Flow cytometry confirmed the presence of the inhibitory receptor NKG2A on expanded duodenal CD8 T cells and HLA-E, the ligand for NKG2A, on expanded aberrant cells. **CONCLUSION:** RCDII is characterized by the simultaneous presence of an activated CD27$^+$PD-1$^+$ memory CD8$\alpha\beta$ T cell subset and CD4 Tregs, suggesting that checkpoint blockade with anti-NKG2A/PD-1 and/or anticytotoxic T lymphocyte antigen 4 may be an attractive treatment option.

Keywords: Coeliac; Gluten enteropathy; Enteropathy-associated T cell lymphoma; Single-cell analysis

Introduction

A minority of patients with celiac disease (CeD) shows refractoriness to a gluten-free diet. Within this patient group, a subpopulation is diagnosed with refractory celiac disease type II (RCDII), based on the presence of a clonally expanded intraepithelial intracellular CD3$^+$ surface CD3$^-$ CD7$^+$CD56$^-$ aberrant cell population in the small intestine. This disease entity is categorized as an indolent lymphoma, with the chance of evolvement into an overt enteropathy-associated T-cell lymphoma. Approximately, 50%–75% of RCDII patients reaches remission upon treatment with cladribine[2] or budesonide;[3] however, upon progression to enteropathy-associated T-cell lymphoma, 5-year survival decreases to 20%.[2]

Most studies on RCDII focused on the aberrant cell population, such as identification of its precursor population,[4,5] genomic drivers[6,7] and phenotypic aspects,[4,7–9] showing genetic and immunophenotypic aberrant cell heterogeneity, reflecting its clinical heterogeneity and the need for patient-tailored medicine.

However, there is a lack of knowledge on other immune cells playing a role in RCDII, such as T lymphocytes, B lymphocytes, and macrophages in the tumor microenvironment (TME). Tumors have been described as dynamic ecological systems[10] and differences within this TME may

Abbreviations used in this paper: **CeD, celiac disease; CTLA-4, cytotoxic T lymphocyte antigen 4; EATL, enteropathy-associated T-cell lymphoma; GSE, gene set enrichment; IF, immunofluorescence; IL, interleukin; NK, natural killer; PB, peripheral blood; PD-1, programmed cell death protein 1; RCDII, refractory celiac disease type II; scRNA-seq, single-cell RNA-sequencing; TME, tumor microenvironment; Treg, T regulatory; tSNE, t-distributed stochastic neighborhood embedding; VA, villous atrophy.**

Most current article

2772-5723
https://doi.org/10.1016/j.gastha.2024.08.023

reflect differences in clinical outcome including response to cancer immunotherapy. This is exemplified by immune 'hot' tumors known for high immune cell infiltrates eg melanoma and lung cancer, responding to cancer immunotherapy such as cytotoxic T lymphocyte antigen 4[11] and programmed cell death protein 1 (PD-1) therapy.[12] To clarify the ecological system in RCDII and options for immunotherapy, it is crucial to characterize the TME in RCDII duodenum.

In this study, we performed an in-depth characterization of innate and adaptive cell subsets by single-cell mass cytometry and single-cell RNA sequencing in RCDII duodenum in comparison with healthy duodenum. For further analysis, we applied immunofluorescence (IF) staining and flow cytometry.

Collectively, we observed a previously unidentified, activated, and potentially cytotoxic $CD27^{+}PD\text{-}1^{+}$ $CD8\alpha\beta$ T cell population as well as an enrichment of CD4 T regulatory (Treg) cells in the lamina propria of RCDII patients. These results are indicative of an immunosuppressive TME and suggest that immune checkpoint blockade may be an attractive treatment option.

Materials and Methods

Human Material

For adult samples the local Medical Ethical Committee (MEC) from Amsterdam, location VU Medical Center, approved this study (protocol 2017.077). For paediatric samples, the MEC from Leiden University Medical Center approved this study (protocol 14.041). Signed informed consent was obtained from collection of human material. This study was performed in accordance with the local ethic guidelines and in accordance with the ethical principles from the Declaration of Helsinki.

Per patient, 2–3 biopsies were collected in Hank's Buffered Salt Solution (HBSS) without calcium and magnesium (Gibco, Thermo Fisher). Blood samples were collected in sodium anticoagulant heparin tubes (BD Vacutainer heparin tubes). For single-cell CyTOF panel 1, from 10 RCDII patients, we obtained fresh small intestinal biopsies (n = 12) with paired peripheral blood (PB) samples (n = 9) (2 patients were included twice); from 6 control patients with healthy duodenal tissue, we similarly obtained fresh small intestinal biopsies (total n = 6) with paired PB samples (n = 6). Moreover, we obtained fresh small intestinal biopsies from adult CeD patients (n = 8), adult RCDI patients (n = 2) and paediatric CeD patients (n = 4) For single-cell CyTOF panel 2, from 5 RCDII patients, we obtained fresh small intestinal biopsies (n = 5 with paired PB samples (n = 5).

Isolation of PBMCs from Peripheral Blood

Peripheral blood mononuclear cells (PBMCs) were isolated from blood samples using density-gradient centrifugation on Ficoll-Amidotrizoate (LUMC pharmacy). Cells were collected by a Pasteur pipette, transferred to 20% fetal calf serum (FCS)/RPMI (Gibco, Thermofisher), washed and collected in preferred solution.

Isolation of Leukocytes from Duodenal Biopsies

First, intraepithelial lymphocytes (IELs) were isolated from duodenal biopsies by treatment with HBSS with 1 mM EDTA (made in-house; J.T. Baker), rolling for 2 × 45 min at 37 °C. IELs were collected in 20%FCS/RPMI and kept at 4 °C. Second, single-cells were isolated from the lamina propria (LP) by 1.5hr incubation with 10 units/mL collagenase IV (Worthington) and 200 μg/ml DNase I grade II (Roche). Next, isolated IELs and LP cells were passed through a 70 μm cell strainer for obtainment of single-cell suspensions. Cells were washed and collected in preferred solution.

Snap-freezing Biopsies

Freshly obtained duodenal biopsies were snap-frozen in OCT using isopenthane (GPR Rectapur, VWR) and stored at −80 °C.

Paraffin-embedded Biopsies

Freshly obtained duodenal biopsies were paraffinized by the pathology department at the LUMC.

Single-Cell Mass-cytometry

Preconjugated metal-labelled antibodies (Abs) were purchased from Fluidigm (San Francisco, California, USA). Selected purified Abs were conjugated in-house with the MaxPar X8 antibody labeling kit (Fluidigm) according to the manufacturer's instructions: CD1a, CD103, CD122, CD15, CD5, CD8b, CD20, CD28, CD45RO, CRTh2, HLA-DR, IgM, KLRG-1, NKp44 and NKp46. These were validated on OneComp beads (Invitrogen) and PBMCs.

After obtainment of single-cell suspensions, cell were once washed with 0.5% FCS/DPBS (Dulbecco's Phosphate Buffered Saline) (Gibco, Thermo Fisher), then washed with staining buffer (Fluidigm) (with 1:250 diluted 0.5 mM EDTA). For identification of dead cells, suspensions were incubated with 1:2000 diluted 2000mM intercalator-103Rh (Fluidigm) 15 min at rT. After wash and incubation with Fc-block (Biolegend), cells were stained with metal-conjugated antibodies for 45 min at rT. Cells were washed 3 times with staining buffer. For identification of nucleated cells, cells were labelled with 1:4000 diluted 500 mM Cell-ID Intercalator-Ir (Fluidigm) in MaxPar Fix and Perm buffer (Fluidigm) overnight at 4 °C. Next day, cells were counted and washed 3 times with staining buffer.

Within 14 days, samples were acquired at Helios mass cytometer (Fluidigm, San Francisco, CA, USA), narrow-bore injector, at the Flow Core Facility (FCF) of the LUMC. Samples were concentrated in MilliQ. For normalization, EQ 4 Elements Calibration beads in 1:10 dilution (Fluidigm, passport number EQ-P13H2302_ver2) were spiked in with each sample. Samples were measured in batches of 2-8 samples per day, all by the same operator. Paired intestinal and blood samples were measured on the same day.

Single-Cell RNA-sequencing

IELs and LP cells were isolated from 7 duodenal biopsies as described above. Single-cell suspensions were treated with red blood cell lysis buffer (LUMC pharmacy) and microbeads for removal of dead cells (Miltenyi Biotec). Using MACS beads (Miltenyi Biotec), we performed positive selection of live CD45+ cells. Single-cell RNA sequencing was performed using 10X Genomics Single Cell system. Samples were sequenced on one run with the NovaSeq 6000 system

(Illumina). Cell Ranger software v2.2.0 was used for preprocessing of obtained data.

Data Analysis

For analysis of single-cell mass cytometry data, first, we gated out duplicates, dead cells, beads and debris using FlowJo v10 Software (Tree Star Inc.). Single live CD45$^+$ cells were checked for consistent Ab staining in FlowJo: inconsistency was observed for CD103, CD20, CD8a and IgM. These markers were used for assignment to major lineages but not for cell clustering in further analysis. Marker expression overlays were used for data interpretation. We used the same approach for analysis of mass cytometry panel 2. Here, we observed inconsistent staining of 7 antibodies namely CD103, CD57, CD8a, CD95, Helios, Perforin and TGF-β. Data of single live CD45$^+$ cells were sample-tagged and arc-sine transformed with cofactor 5, using Cytosplore software $^{+\text{HSNE}}$.[13,14] HSNE embedding in Cytosplore were performed using perplexity 30, iterations 1000. Cells assigned to an incorrect lineage were transferred before further analysis.

For analysis of single-cell RNA sequencing data, Seurat package v3.1.1[15] was used in R version 4.0.1. The preprocessed dataset of live CD45+ cells was setup in an Seurat object and raw data matrices were merged, which included addition of a cell identifier for tracing the origin of a particular cell. Data were filtered: each gene was expressed in $\geq$ 3 cells and $\geq$ 200 genes were expressed per cell; cells with unique gene cell counts $<$ 200 and $>$ 5000 and a mitochondrial gene percentage of $>$ 25. Filtered data were log-normalized, scaled and unwanted sources of variation were removed. PCA-analysis was performed based on the 2000 most variable genes, selected using the vst method. For graph-based clustering, 18 PCA dimensions were used with a resolution of 1.1. Clusters were visualized with a UMAP algorithm.

For analysis of CD8 and CD4 T cells, we performed computational sorting from the dataset of duodenal CD45+ cells. Separately, we performed computational sorting for analysis of aberrant cells. For each computational sorting, we used 20 PCA-dimensions for reclustering; clusters were visualized with a UMAP algorithm.

For gene set enrichment (GSE) and biological pathway analysis, we used the reference gene dataset 'Molecular Signatures Database Hallmark Gene Set Collection'.[16,17]

Immunofluorescence Staining on Frozen Tissue

Snap-frozen biopsies were cut using the Leica CM3050 S Research Cryostat. 5μm tissue sections were obtained, placed on silane-coated glass slides (VWR, Radnor, PA, USA), and dried 30–60 min at rT. Sections were fixated for 5 min at -20 °C with methanol, placed in 1x PBS at rT and blocked with Superblock for 30 min at rT. Excess superblock was removed and replaced with diluted primary antibody (PD1, clone 1,015,846, CAT#-mab10864, R&D), followed by a 1 hour incubation at rT. After primary staining, sections were washed with 1x PBS-tween (0,05%) and incubated with poly-HRP for 30 min at rT. After secondary staining, sections were washed again and incubated with Opal520 (Akoya Biosciences) for 60 min in the dark at rT. Sections were boiled in 1x citrate buffer (10 mM, pH 6) for 15 min and allowed to cool down for $\pm$ 60 min. Sections were washed again and incubated with the second primary antibody (CD8, clone D8A8Y, CAT#85336S, CST), followed by o/n incubation at 4 °C in a humidity chamber. Next day, sections were washed again and incubated with the second secondary antibody (donkey anti rabbit AF647, CAT#A31571, Invitrogen) for 60 min at rT in the dark. Afterwards the slides were washed again and stained with DAPI for 15 min at rT in the dark. Finally, sections where mounted using ProLong Gold Antifade Reagent (CAT#9071, CST).

Immunofluorescence Staining on FFPE

Formalin-fixed paraffin-embedded (FFPE) tissues were cut using a microtome. 4 μm tissue sections were obtained, placed on silane-coated glass slides and dried o/n at 37 °C. Sections were deparaffinated using a xylol followed by decreasing concentrations of ethanol. For antigen retrieval, sections were boiled in 1x citrate buffer (10 mM, pH 6) for 10 min and allowed to cool down for $\pm$ 60 min. Further staining followed the same protocol as for frozen tissue samples. The following antibodies were used: first primary antibody (FoxP3, clone: 236A/E7, CAT# 14-4777-82, Invitrogen), second primary antibody (CD4, clone EPR6855, CAT#ab133616, Abcam), first secondary antibody Opal520 (Akoya Biosciences), second secondary antibody (goat anti rabbit CF555, CAT#20035, Biotium) and staining with DAPI.

Data Analysis of Immunofluorescence Stains

Stained tissues were analyzed using QuPath digital image analysis.

Sorting and Expansion of Duodenal Cells

RCDII duodenal biopsy was directly put in tissue-culture in IMDM medium (Gibco) with irradiated allogeneic feeder cells along with 1μg/mL phytohemagglutinin (PHA), 100 IU/mL interleukin (IL)-2 (Chiron) and 10 ng/mL IL-15 (R&D Systems Europe). At day six, we performed flow cytometric surface staining with the following antibodies: CD45-APC-R700 (clone HI30, BD Horizon), CD3-AmCyan (clone SKY7, BD Pharmingen), CD7-V450 (clone M-T701, BD), CD8-BV650 (clone RPA-T8, BD Horizon), CD56-PE (clone MY31, BD Pharmingen), CD4-PE (clone SK3, BD Pharmingen) and TCR$\gamma\delta$-PE (clone 11F2, BD). Subsequently, cells were sorted using an FACSAria flow cytometer (BD Biosciences) and analysed using FACSDiva software (BD Biosciences). We sorted CD45$^+$CD3$^-$CD7$^-$(CD56$^-$) and CD45$^+$CD3$^+$CD8$^+$(CD4$^-$TCR$\gamma\delta^-$) cells. After sorting, we expanded the cells in IMDM medium containing 10% normal human serum (NHS) with 100 IU/mL IL-2 (Chiron) and 10 ng/mL IL-15 (R&D Systems Europe) for CD8 T cells and expanded with 10ng/mL IL-15 for CD3$^-$CD7$^+$CD56$^-$ cells.

Flow Cytometry

For surface flow-cytometric analysis of target molecules on expanded CD3$^+$CD8$^+$ and surface CD3$^-$intracellular CD3$^+$CD7$^+$ cells, the following antibodies were used in several experiments: CD8-PE/Cy7 (clone RPTA-T8, Biolegend), CD3-BV510 (clone UCHT1, Biolegend), CD27-BV650 (clone M-T271, BD Biosciences), PD-1-APC (clone EH12.2H7, Biolegend), NKG2A-PE (clone Z199, Beckman Coulter), NKG2C-BV421 (clone 134,591, BD Biosciences), CD70-PE (clone 113-16, BioLegend) and HLA-E-BV421 (clone 3D12, BioLegend). Cells were first incubated with Human TruStain FcX (Biolegend) for 10min at

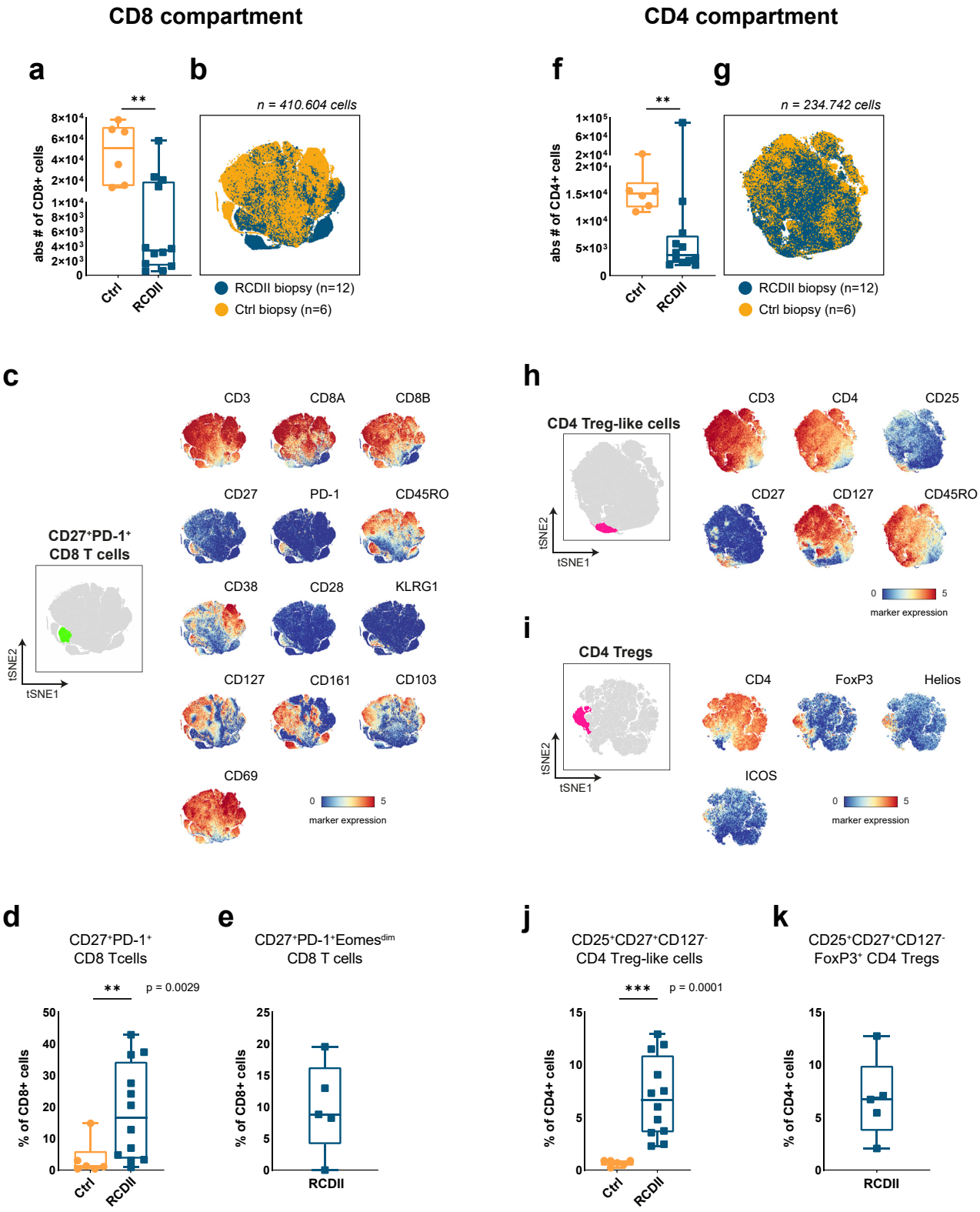

Figure 1. Enrichment of CD27^{+}PD-1^{+} memory CD8$\alpha\beta$ T cells and CD4 Treg-like cells in RCDII duodenum. (A) Absolute counts of CD8 T cells in the mass cytometric dataset, derived from control (n = 6) and RCDII (n = 12) duodenal biopsies. (B) tSNE embedding of CD8 T cells showing 410.604 cells, derived from control (277.219 cells) and RCDII (133.385 cells) duodenal biopsies. (C) tSNE embedding similar as depicted in B) emphasizing a CD27^{+}PD-1^{+} CD8 T cell subset along with marker expression overlays. (D) Frequency of CD27^{+}PD-1^{+} cells in control and RCDII biopsies within the CD8 T compartment. (E) Frequency of CD27^{+}PD-1^{+}Eomes^{dim} CD8 T cells in RCDII biopsies within the CD8 T compartment. (F) *Absolute* counts of CD4-T cells in the mass cytometric dataset, derived from control (n = 6) and RCDII (n = 12) duodenal biopsies. G) tSNE embedding

RT, stained with LIVE/DEAD Fixable Blue (Invitrogen) for 30min at 4 °C, followed by the described antibodies for 30min at 4 °C. Cells were washed and fixated using the Foxp3/Transcription Factor Staining Buffer Set (Invitrogen) according to the manufacturer's instructions. Cells were finally acquired on a 5-laser Cytek Aurora spectral flow cytometer (Cytek Biosciences). UltraComp eBeads (Invitrogen) were used to record single-stains.

Statistics

Data represented in box plots were presented as median ± IQR-range. Group comparisons were performed using 2-tailed Mann-Whitney U tests in GraphPad Prism v9. Spearman correlation analysis (2-tailed) was performed in GraphPad Prism v9 software.

Access to Data

All authors had access to the study data and had reviewed and approved the final manuscript.

Results

Enrichment of CD27$^+$PD1$^+$ Memory CD8αβ T Cells and CD4 Treg-like Cells in RCDII Duodenum

To explore the immune compartment in RCDII duodenum, we applied a mass cytometric antibody panel designed for analysis of 39 cell surface markers on single cell suspensions prepared from RCDII (n = 12) and control (n = 6) biopsies (Table A1), as described previously.[9] The data (Methods) were analyzed using Cytosplore^{+HSNE}[13,14] to identify the major immune lineages.[9] Here, the CD8 compartment contained 410.604 CD8 T cells, with a median number of 3148 cells captured per RCDII biopsy (Figure 1A and B), significantly less than in controls (**P = .0047). Next, we employed t-distributed stochastic neighborhood embedding (tSNE) in Cytosplore[13] to determine the heterogeneity within the CD8 T cell compartment. Marker expression overlays of this tSNE embedding are depicted in Figure 1C.This revealed the presence of a CD27$^+$PD-1$^+$CD45RO$^+$ memory CD8 T cell population (Figure 1C) that constituted up to 43% of the duodenal CD8$^+$ compartment in RCDII, whereas they were virtually absent in controls (**P = .0029, Figure 1D). These CD27$^+$PD-1$^+$ CD8 T cells displayed expression of CD69, consistent with tissue residency, CD38, and variable expression of CD28 and KLRG1 (Figure 1C). Moreover, this population lacked expression of CD127 (IL-7 receptor), CD161 and CD103, the latter suggesting residence in the lamina propria (Figure 1C). To validate these findings we applied a second mass cytometry antibody panel for analysis of 42 surface and intracellular markers, as described previously,[9] to single cell suspensions prepared from biopsies of 5 additional RCDII patients (CyTOF dataset 2) (Table A1), which likewise showed the presence of this CD27$^+$PD-1$^+$ CD8 T cell subset (Figure 1E). In contrast, we observed that CD27$^+$PD-1$^+$ CD8 T cells were absent in duodenal tissue from CeD (adults and children; active and nonactive disease) and RCDI patients (Table A1; Figure A1A).

Next, we performed a tSNE analysis of the duodenal CD4 compartment (234.742 cells in total) which showed a median number of 14.700 cells in controls vs 4000 cells in RCDII (**P = .0069, Figure 1F and G)). Virtually all CD4 T cells displayed a CD45RO$^+$ memory phenotype (Figure 1H). In RCDII, higher frequencies of CD25$^+$CD27$^+$CD127$^{dim/-}$CD4 Treg-like cells (median 6.7% [3.6-10.8]) were observed compared to controls (***P = .0001 (exact), Figure 1H and J). Analysis of the CD4 compartment in CyTOF dataset 2 demonstrated expression of FoxP3 and Helios (Figure 1I) by the CD25$^+$CD27$^+$CD127 $^{dim/-}$CD4 T cells in a similar frequency (median 6.7% [3.8-9.9], Figure 1K), confirming the Treg-like phenotype. Additionally, we observed differential expression of ICOS (Figure 1I). Lastly, we observed higher numbers of CD25$^+$CD27$^+$CD127 $^{dim/-}$ CD4 Treg-like cells in part of the CeD patient group, predominantly in patients with active disease (>5% of total CD4 T cells) (Figure A1B).

Together this analysis demonstrates enrichment of CD27$^+$PD-1$^+$CD45RO$^+$ memory CD8 T cells and CD4 Tregs in RCDII when compared to controls.

Confirmation of the Presence of Cytotoxic CD27$^+$PD-1$^+$ CD8αβ T-Cells and FoxP3$^+$ CD4 Tregs in a Single-cell RNA-sequencing (scRNA-seq) Dataset

Next, we assessed the presence of CD27$^+$PD-1$^+$ memory CD8αβ T-cells and FoxP3$^+$ CD4 Tregs in a scRNA-seq dataset of duodenal CD45$^+$ cells from an RCDII patient (RCDII-12, Table A1).[9] We computationally selected the CD8 and CD4 T cells (Methods) and observed that 2 populations of CD8 cells (CD8-1 and CD8-2) and 2 populations of CD4 T cells (CD4-1 and CD4-2) could be distinguished (Figure 2A).

of CD4 T cells showing 234.742 cells, derived from control (91.953 cells) and RCDII (142.789 cells) duodenal biopsies. (H) tSNE embedding similar as depicted in (F) emphasizing a CD25$^+$CD27$^+$CD127$^{dim/-}$ CD4 Treg-like cell subset along with marker expression overlays. (I) tSNE embedding of CD4 T cells from the second mass cytometric dataset, emphasizing the presence of CD4$^+$FoxP3$^+$ Tregs along with marker expressing overlays. (J) Frequency of CD25$^+$CD27$^+$CD127 $^{dim/-}$ CD4 Treg-like cells in control and RCDII biopsies within the CD4 T compartment. (K) Frequency of CD25$^+$CD27$^+$CD127 $^{dim/-}$FoxP3$^+$ CD4 Tregs in RCDII biopsies within the CD4 T compartment. (C,H-I) Arcsine transformed data resulting in median marker expression values, ranging from 0 to 5 (blue to red). (A, D, F, J) Significance was calculated using the Mann-Whitney test. **$P \leq .01$, ***$P \leq .001$. Plots represent median ± interquartile range.

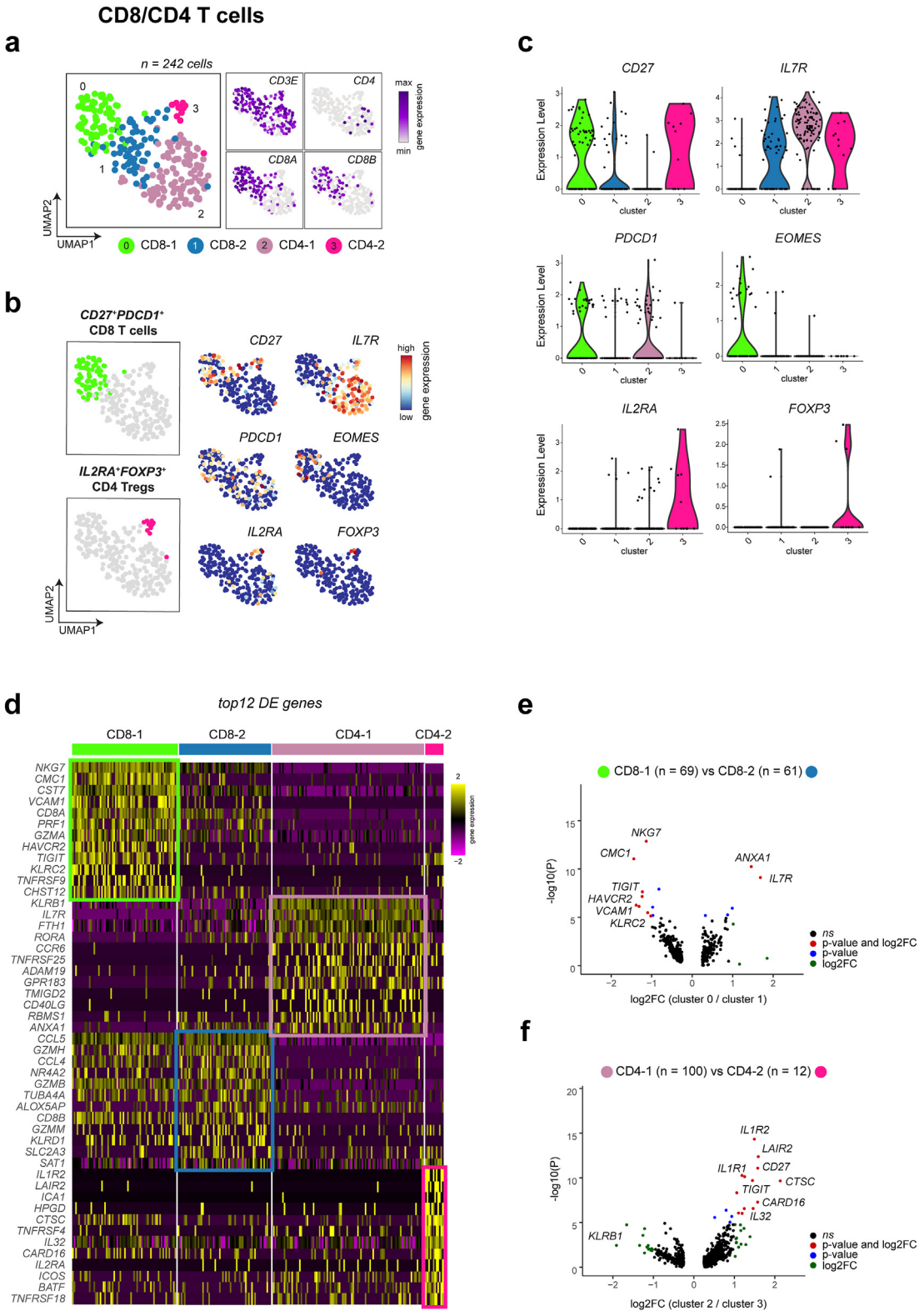

Figure 2. Confirmation of cytotoxic CD27$^+$PD-1$^+$ CD8$\alpha\beta$ T-cells and FoxP3$^+$ CD4 Tregs with immunosuppressive features in a scRNA-seq dataset. (A) UMAP embedding showing 242 duodenal CD8 and CD4 T cells, computationally sorted from a dataset of CD45$^+$ duodenal cells derived from patient RCDII-12. Clustering resulted in 4 cell clusters: two CD8 T (cluster 0, n = 69 cells; cluster 1, n = 61 cells) and two CD4-T cell clusters (cluster 2, n = 100 cells; cluster 3, n = 12 cells). Gene expression overlays for UMAP embedding showing normalized single-cell gene expression data of immune lineage markers. Color bar from grey (minimum) to purple (maximum). (B) UMAP embedding similar as depicted in (A), emphasizing cell cluster containing *CD27$^+$PDCD1$^+$* cells (CD8-1) and *IL2RA$^+$FOXP3$^+$* cells (CD4-2). Gene expression overlays UMAP embedding showing

For the identification of CD27$^+$PD-1$^+$ CD8 T cells and CD4 Tregs, discriminative markers were plotted onto the UMAP plot (Figure 2B). Consistent with the mass cytometry data we detected expression of *CD27*, *PDCD1* (PD-1) and *EOMES* in CD8 T cells, with higher expression of these markers in the CD8-1 population (Figure 2A–C). Moreover, the CD8-1 population lacked gene expression of *IL7R* (CD127). The CD4-2 T cell population displayed expression of *IL2RA* (CD25) and *FOXP3* (Figure 2A–C), consistent with the mass cytometry data and confirming the presence of CD4 Tregs in RCDII duodenum.

We next analyzed the top 12 differentially expressed genes in these four cell populations, revealing that the most discriminative markers for the *CD27*$^+$*PDCD1*$^+$ CD8 T cell population were *CMC1* (COX assembly mitochondrial protein) and *VCAM1* (Figure 2D). Moreover, we observed expression of cytolytic proteins *NKG7, PRF1* and *GZMA,* as well as *KLRC2*, representing NKG2C, an activating receptor interacting with HLA-E. Lastly, *HAVCR2* (TIM-3), *TIGIT* and *TNFRSF9* (CD137), markers associated with immunoregulatory properties were expressed in the CD8-1 population.

Within the CD4 T cell clusters, we observed that CD4-1 was an *CD40LG*$^+$ activated CD4 T cell population, of which most cells showed *IL7R*$^+$*KLRB1*$^+$ (Figure 2D) expression which correlates with CD127$^+$CD161$^+$ CD4 T cells defining the largest CD4 subset in the mass cytometry data (Figure 1G). *FOXP3*$^+$*IL2RA*$^+$ (CD25) Treg cells (CD4-2) expressed cytokine-related genes *IL1R2* and *IL32,* costimulatory genes *TNFSRS4* (OX40) and *ICOS* and the transcription factor *BATF.* Lastly, expression of *TIGIT*[18] and *TNFRSF18* (GITR) was consistent with the Treg phenotype[19] (Figure 2D).

Finally, we assessed the most discriminative markers between the two CD8 (Figure 2E) and two CD4 T cell populations (Figure 2F). In addition to the genes displayed by the top 12 differentially expressed analysis, this revealed that *CD27*$^+$*PDCD1*$^+$ CD8 T cells could best be discriminated by the lack of *IL7R* and *ANXA1* (Annexin 1) while expression of *CD27* was an additional marker for *FOXP3*$^+$*IL2RA*$^+$ CD4 Treg cells.

Altogether, these results are in line with the mass cytometry data and demonstrate the presence of an *CD27*$^+$*PDCD1*$^+$*IL7R*$^-$ CD8 T cell population with cytolytic properties and *IL2RA*$^+$*FOXP3*$^+$ CD4 Tregs with immunosuppressive features in RCDII duodenum.

PD-1$^+$CD8$^+$ T Cells and CD4 Tregs are Located in the Lamina Propria of RCDII Patients

To visualize the distribution of activated PD-1$^+$ CD8 T lymphocytes in RCDII duodenum, we performed IF staining, targeting CD8 and PD-1 on snap-frozen RCDII duodenum biopsies (Methods). We applied this staining to tissue from 2 RCDII patients in which 37%–43% of the CD8 T cells displayed the CD27$^+$PD-1$^+$ phenotype, as observed in the single-cell mass cytometry analysis (Figure 1D and E). For comparison, we analyzed tissue from controls and CeD patients with active disease (confirmed villous atrophy). In Figure 3A the individual CD8 and PD-1 stains as well as the overlay of the stains are shown in RCDII tissue, which identifies an abundance of PD-1$^+$CD8$^+$ cells. Similarly, PD-1$^+$CD8$^+$ cells, although in lower abundance, were detected in a second RCDII sample (Figure 3B), whereas these cells were absent in the healthy and CeD duodenum samples (Figure 3C and D). Moreover, we observed that the PD-1$^+$CD8$^+$ cells resided in the duodenal lamina propria (Figure 3A and B), in agreement with the lack of expression of CD103 (Figure 1C).

Similarly, we performed IF staining for detection of FoxP3$^+$ CD4 Tregs in RCDII duodenum. Hereto, we applied FoxP3 and CD4 staining on paraffin-embedded duodenal biopsies (Methods). This staining was performed on tissue from 3 RCDII patients in which we observed the highest frequencies (±12%) of CD25$^+$CD27$^+$CD127$^{dim/-}$ CD4 Treg-like cells in the mass cytometric analysis (Figure 1J and K) and on tissue from controls and CeD patients (confirmed villous atrophy). In Figure 4, representative images are displayed of two RCDII tissues (Figure 4A and B), one control (Figure 4C) and one CeD patient (Figure 4D). These images show enrichment of FoxP3$^+$CD4$^+$ cells in the lamina propria of RCDII, whereas they were virtually absent in control and CeD tissue. Thus, similar to PD-1$^+$CD8$^+$ cells, FoxP3$^+$CD4$^+$ cells reside in the lamina propria of RCDII patients.

Enrichment of CD4 Treg-like Cells in Peripheral Blood of RCDII Patients

Next, we set out to determine whether T cells displaying a phenotype similar to that observed on CD4 Tregs and CD27$^+$PD-1$^+$ memory CD8 T cells in RCDII patients could be detected in PB.

Simultaneous with staining of duodenal single cell suspensions, we applied the mass cytometric panel on peripheral blood mononuclear cells (PBMCs) prepared from RCDII (n = 9) and control (n = 6) samples, as described previously.[9] In alignment with data analysis in duodenal biopsies, we applied Cytosplore^{+HSNE}[13,14] for analysis.

We observed enrichment of CD25$^+$CD127$^{dim/-}$CD27$^+$ CD4 Treg-like cells (median 9.5% [6.7-14.7]) (**$P = .0048$) in PB of RCDII patients compared to controls (Figure 5A),

normalized single-cell gene expression data. Color bar from blue (low) to red (high). (C) Violin plots showing log-normalized gene expression data per cluster of selected genes, similar as in (A, B). (A-C) Colors and numbers indicate distinct cell clusters. (D) Heatmap showing the top differentially expressed (DE) genes in each cluster, as normalized dispersions of single-cell gene expression data (z-score, color bar from purple to yellow). (E) Volcano plot showing genes that significantly differ between cell subsets CD8-1 and CD8-2. (F) Volcano plot showing genes that significantly differ between cell subsets CD4-1 and CD4-2.

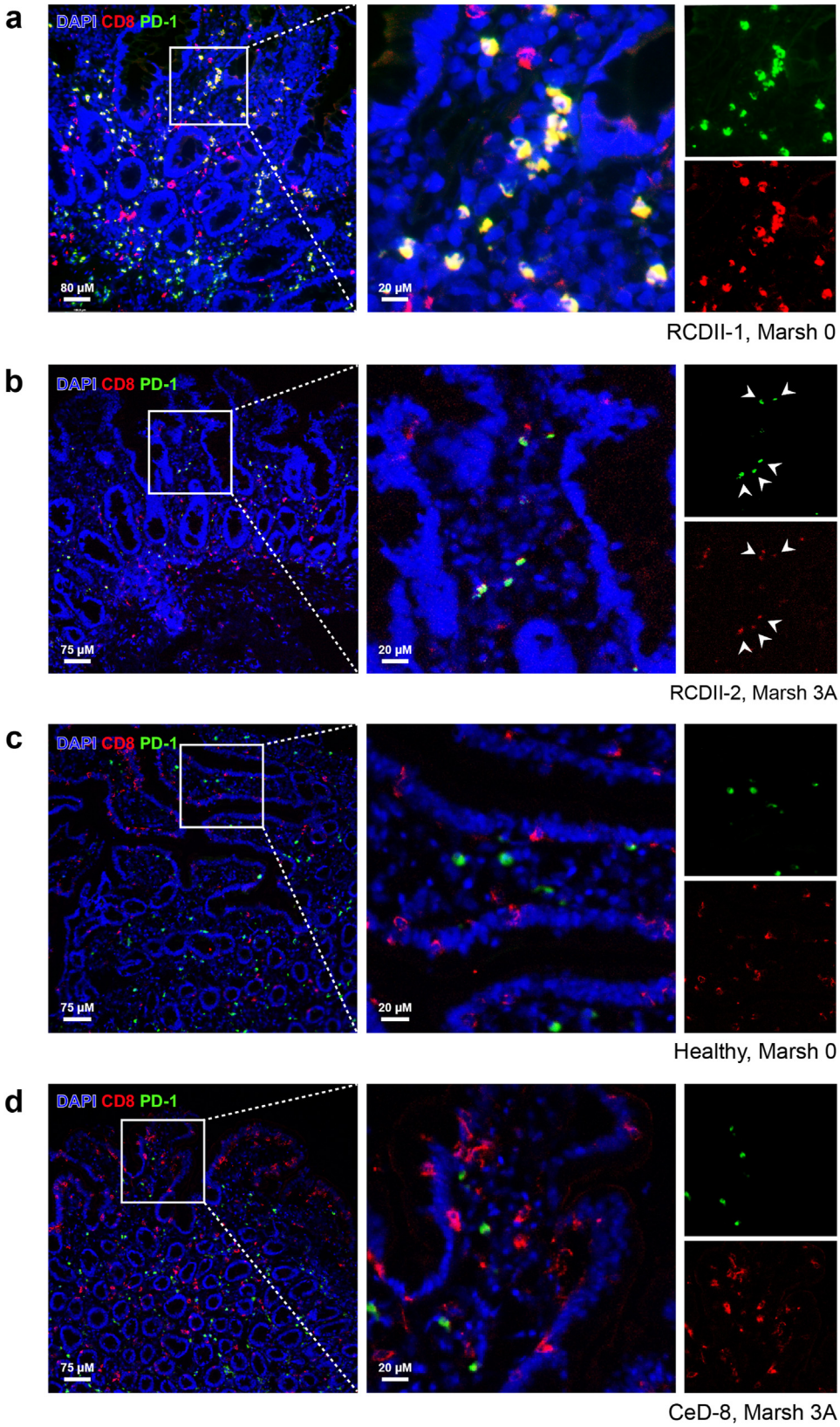

Figure 3. Higher cell counts of PD-1^{+}CD8^{+} cells in the lamina propria of RCDII patients. (A-D) Representative images of immunofluorescent detection of PD-1^{+}CD8^{+} cells (colored yellow) in duodenal tissues from (A) RCDII patient without villous atrophy (VA) (RCDII-1) (B) RCDII patient with VA (RCDII-2) (C) healthy control duodenum (D) CeD patient with VA. (A-D) Displayed are DNA (blue color), PD-1 (green color) and CD8 (red color) staining. For each tissue, we show overview images (75–80μm) and representative enlarged regions (20μm) together with single stains for PD-1 and CD8. (B) Arrows indicate cells with double expression of CD8 and PD-1.

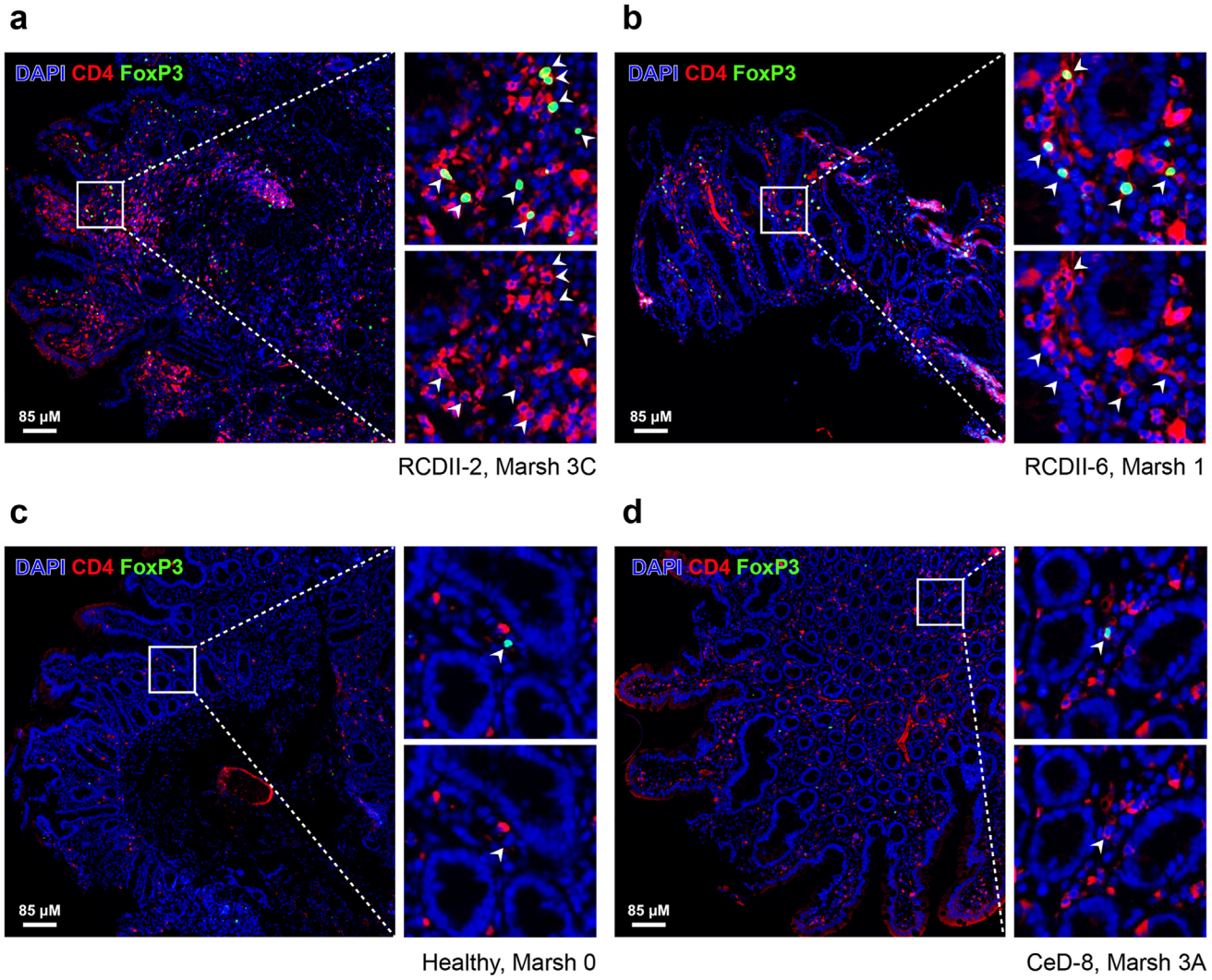

Figure 4. FoxP3^{+}CD4^{+} cells located the lamina propria of RCDII patients. (A-D) Representative images of immunofluorescent detection of FoxP3+CD4+ cells in duodenal tissue from (A) RCDII patient with villous atrophy (VA) (RCDII-2). (B) RCDII patient without VA (RCDII-6) (C) healthy control duodenum. (D) CeD patient with VA (A-D) Displayed are DNA (blue color), FoxP3 (green color) and CD4 (red color) staining. For each tissue, we show overview images (85μm) and representative enlarged regions. Arrows indicate cells with double expression of FoxP3 and CD4.

while this was not the case for CD27^{+}PD-1^{+} CD8 T cells (Figure 5B).

Gene Set Enrichment and Biological Pathway Analysis Identifies Activator and Effector Properties of the CD27^{+}PDCD1^{+} CD8 T Cell Population

To assess functionality of the *CD27^{+}PDCD1^{+}* CD8 T cell population (Figure 2), we performed a GSE analysis[16] (Methods). This analysis revealed significant enrichment of several CD8-related pathways: PD1^{high} CD8 T cell (Figure 6A), memory CD8 T cells (Figure 6B), and effector CD8 T cells (Figure 6C). Furthermore, the *CD27^{+}PDCD1^{+}* CD8 T cells displayed a phenotype more similar to effector CD8 T cells rather than an exhausted phenotype (Figure 6D). Although we did not detect cytotoxic pathways in the reference datasets, cytotoxic gene signatures (*PRF1*, *GZMK* and *GMZB*) were observed within the enriched pathways.

Additionally, we performed a biological pathway analysis on the top 500 upregulated unique genes from the *CD27^{+}PDCD1^{+}* CD8 T cell population (Table A2). The most significantly enriched pathways of interest were the 'T cell activation pathway' (ranked 1), the 'natural killer cell mediated cytotoxicity' (ranked 22), 'leukocyte mediated cytotoxicity (ranked 29) and leukocyte proliferation (ranked 40).

In conclusion, this GSE and biological pathway analysis shows that the *CD27^{+}PDCD1^{+}* CD8 population displays an activated/effector memory profile.

Presence of Potential Immunotherapeutic Targets on CD27^{+}PD-1^{+} CD8 T Cells

The most powerful cells for targeting tumors are CD8 T cells. We therefore aimed at identification of potential

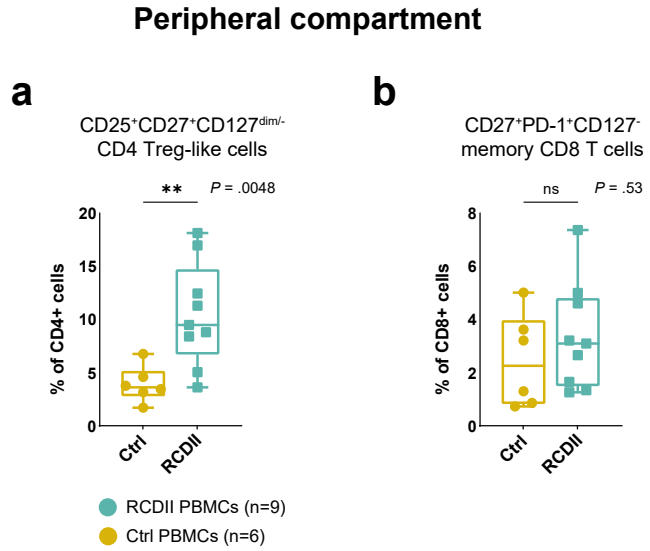

Figure 5. Enrichment of CD4 Treg-like cells in peripheral blood of RCDII patients. (A) Frequency of $CD25^{+}CD27^{+}CD127^{dim}$ CD4 Treg-like cells as percentage of CD4 T cells in peripheral blood (PB) of control and RCDII patients. (B) Frequency of $CD27^{+}PD\text{-}1^{+}CD127^{-}$ memory CD8 T cells as percentage of CD8 T cells in PB of control and RCDII patients. (A, B) Significance was calculated using Mann-Whitney test. $^{**}P \leq .01$. Plots represent median ± interquartile range.

immunotherapeutic targets expressed by the observed $CD27^{+}PD\text{-}1^{+}$ CD8 T cell population. First, we screened the duodenal scRNA-seq dataset. For comparison, we took along CD4 populations in the analysis (Figure 7A and B). On the *$CD27^{+}PDCD1^{+}$* CD8 T cell population, we observed the expression of immune checkpoint molecules *HAVCR2* (TIM-3), *TIGIT, TNFRSF9* (CD137) and *KLCR2* (NKG2C) (Figure 2D). Besides *KLRC2 (*NKG2C) (Figure 7C), gene expression of *KLRC1* (NKG2A) (Figure 7C) and *KLRD1* (CD94) was observed on part of the *$CD27^{+}PDCD1^{+}$* CD8 T cell population.

While the NKG2C/CD94 dimer forms an activating receptor, NKG2A/CD94 is an inhibitory receptor. We therefore wanted to confirm the expression of NKG2A and NKG2C at the protein level. Hereto, we sorted and expanded CD8 T cells from an RCDII duodenal biopsy (Methods). These expanded CD8 T cells displayed a resident ($CD69^{+}$) memory ($CD45RO^{+}$) phenotype and expression of $CD27^{+}$ and $PD\text{-}1^{+}$, consistent with the *ex vivo* phenotype. We confirmed expression of NKG2A, whereas protein expression of NKG2C was not observed (Figure 7D).

Next, we examined for ligands of NKG2A, CD27 and PD-1 on aberrant cells in the scRNA-seq dataset, HLA-E, CD70 and PD-L1, respectively. Hereto, we computationally selected aberrant cells/NK cells (Methods), resulting in a dataset of 643 cells (Figure 7E) containing 424 aberrant cells (Figure 7F). We confirmed the presence of *HLA-E* and *CD70* on aberrant cells in the scRNA-seq dataset (Figure 7G), whereas virtually no *CD274* (PD-L1) was detected. To confirm protein expression of these molecules on aberrant cells, we performed flow cytometric staining on sorted and expanded aberrant $Lin^{-}CD3^{-}CD7^{+}CD56^{-}$ cells from an RCDII duodenal biopsy (Methods). This confirmed HLA-E and CD70 protein expression (Figure 7H).

Collectively, this screening shows potential for interactions between the activated CD8 T cells and aberrant cells, via the NKG2A:HLA-E axis and the CD27-CD70 T-cell costimulatory pathway.

Discussion

In this study, we used single-cell mass cytometry, scRNA-seq, IF staining and flow cytometry for characterization of the immune composition in the TME of RCDII duodenal samples.

First, we applied single-cell phenotypic and transcriptional analysis of the CD8 compartment. Herein, we observed a previously unidentified population of $CD27^{+}IL7R^{-}$ memory CD8$\alpha\beta$ T cells in RCDII duodenum, characterized by expression of PD-1 and Eomes. *In situ* analysis showed localization of $PD\text{-}1^{+}CD8^{+}$ cells in the lamina propria of RCDII patients. Single-cell RNA sequencing data confirmed the presence of this $CD27^{+}IL7R^{-}$ memory CD8 T cell population and showed activated/effector properties along with expression of cytolytic molecules (*GZMH, GZMK, NKG7*) and immune checkpoints (*HAVCR2* (TIM-3), *TIGIT* and *TNFRSF9* (CD137)).

In the context of RCDII, there is a lack of knowledge on putative CD8-mediated antitumor responses. With the discovery of this activated $CD27^{+}PD\text{-}1^{+}$ memory CD8 T cell subset, we hypothesized these cells might harbor cytotoxic action against aberrant cells. Despite low CD8 T cell frequencies in RCDII duodenum, we noted an expansion of this activated CD8 T cell subset. This subset may also indicate a state of hyporesponsiveness, induced by chronic inflammation in the duodenal RCDII microenvironment, leading to diminished antitumor activity in RCDII.[20] The absence of higher frequencies of the $CD27^{+}PD\text{-}1^{+}$ memory CD8 T cell subset in PB suggest tissue-residency, as indicated by the expression of CD69 in the duodenum. We observed no correlation with clinical features such as symptoms, Marsh scores and aberrant cells, which possibly can be attributed to heterogeneity of RCDII.[9]

In more than 50% of the RCDII patients, aberrant cells harbor a high number of nonsynonymous mutations.[6,7] It is known that tumors with a high mutational burden serve as a reservoir of highly immunogenic tumor neoantigens, responsive to immunotherapy. Thus, it is tempting to speculate that aberrant cells in RCDII express neoantigen that may be the target of the identified resident CD8 T cells. Unfortunately, we were unable to evaluate the cytolytic potential of the CD8 T cells towards the aberrant cells due scarcity of the biopsy material. This remains to be investigated in future studies.

Moreover, we observed expression of the inhibitory receptor NKG2A on CD8 T cells, suggesting a potential interaction via the NKG2A:HLA-E axis. This is supported by the

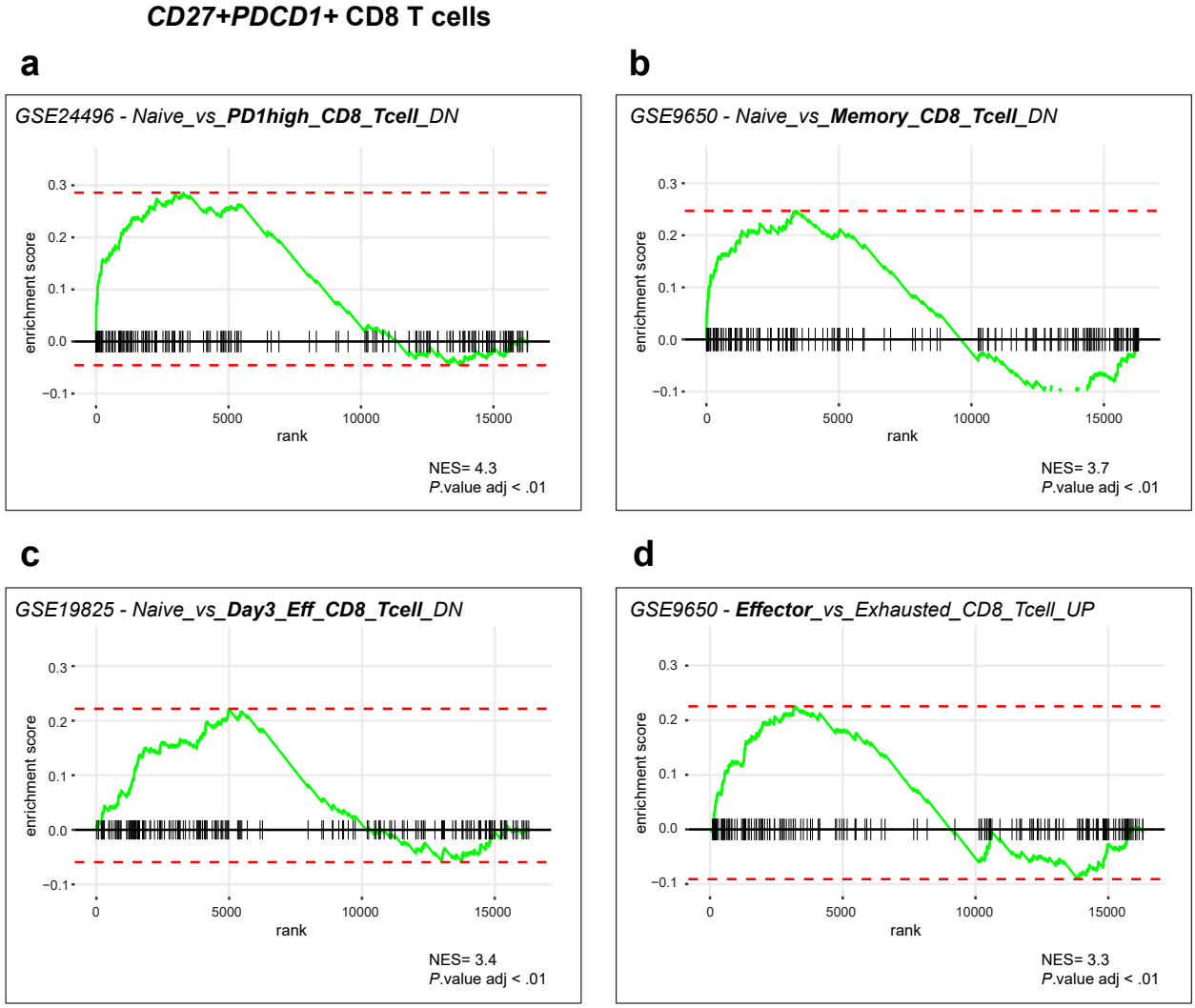

Figure 6. Gene set enrichment (GSE) analysis identifies activator and effector properties of the *CD27*$^{+}$*PDCD1*$^{+}$ CD8 T cell population. (A-D) GSE analysis results plotted by position in the ranked list of genes (rank, x-axis) and running enrichment score (y-axis). *P*.value adj. represents Benjamini-Hochberg adjusted *P* value that accounts for multiple testing.

presence of HLA-E on sorted duodenal aberrant cells and by the documented upregulation of NKG2A following the acquisition of PD-1 on tumor-infiltrated CD8 T cells.[21] Importantly, NKG2A was recently discovered to be an immune checkpoint for NK cells and CD8 T cells.[22] Secondly, we investigated the role of the CD27-CD70 T cell costimulatory pathway, finding constitutive expression of CD70 on RCDII aberrant cell lines. Constitutive CD70 expression in cancer is described for its role in tumor evasion and tumor progression, by a negative feedback loop on tumor CD8 T cells.[23–25] Moreover, constitutive CD27-CD70 engagement promotes survival and expansion of CD4 Tregs, which fits within the observed data.[24] Together, this points toward multiple inhibitory signals on CD8 T cells in RCDII that may be overcome by immune checkpoint blockade.

Next to detection of an activated CD8 T cell subset, we observed an increased presence of immunosuppressive CD25^{+}CD27^{+}CD127 $^{dim/-}$FoxP3^{+} CD4 Tregs in RCDII duodenum. Enrichment of CD4 Tregs was also observed in PB of RCDII patients, in agreement with a previous study showing higher frequencies of circulating FoxP3^{+} Tregs in RCD type I and type II.[26] Although the presence of CD4 Treg-like cells was predominantly observed in patients with active CeD vs nonactive CeD, not all patients with active disease displayed higher frequencies of CD4 Tregs. Thus, these data were inconclusive in determining whether active disease in CeD, associated with an immunosuppressive environment, contributes to clonal expansion of aberrant IELs.

Collectively, our observations point to a suppressive tumor-microenvironment in RCDII in the context of CD4 and CD8 T cell populations. This is consistent with findings of a previous study from our laboratory,[9] where we documented the presence of immunosuppressive M2 macrophages populating the lamina propria of RCDII patients (ie tumor-associated macrophages). Moreover, this study

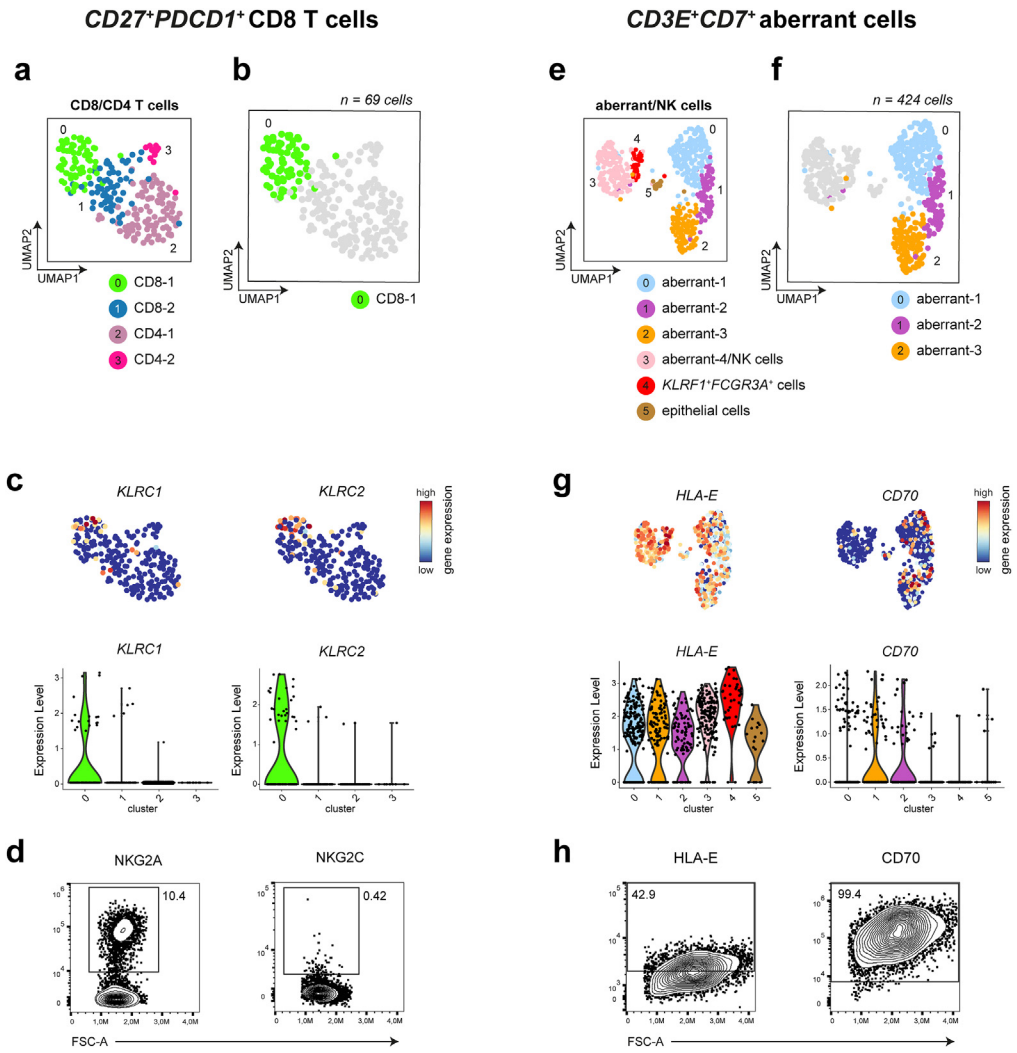

Figure 7. Presence of potential immunotherapeutic targets on duodenal CD8 T cells. (A) UMAP embedding showing 242 duodenal CD8 and CD4 T cells, divided in 4 cell clusters: two CD8 T (cluster 0 and 1) and two CD4-T cell clusters (cluster 2 and 3). (B) UMAP embedding similar as depicted in A), emphasizing cell cluster CD8-1 (n = 69 cells), representing *CD27*$^{+}$*PDCD1*$^{+}$ CD8 T cells. (C) Gene expression overlays for UMAP embedding depicted in (A,B) showing log-normalized gene expression data for *KLRC1* (NKG2A) and *KLRC2* (NKG2C), together with violin plots showing log-normalized gene expression per cluster for *KLRC1* and *KLRC2*. (A-C) Colors and numbers indicate distinct cell clusters. (D) Flow cytometry data displaying expression data of NKG2A and NKG2C on sorted duodenal RCDII CD8 T cells. (E) UMAP embedding showing 643 duodenal aberrant cells, aberrant/NK cells, *KLRF1*$^{+}$*FCGR3A*$^{+}$ cells and epithelial cells. (F) UMAP embedding similar as depicted in (E), emphasizing cell cluster aberrant-1 (n = 214 cells), aberrant-2 (n = 122 cells) and aberrant-3 (n = 88 cells), representing aberrant cells (total n = 424 cells). (G) Gene expression overlays for UMAP embedding depicted in (E, F) showing log-normalized gene expression data for *HLA-E* and *CD70*, together with violin plots showing log-normalized gene expression per cluster for *HLA-E* and *CD70*. (C, G) Color bars showing gene expression from blue (low) to red (high) expression. (H) Flow cytometry data displaying expression data of HLA-E and CD70 on sorted duodenal RCDII aberrant cells.

demonstrated a lack of CD45RA^{+}CD56^{+} NK cells among most RCDII patients, which play a relevant role in cytolytic NK cell-mediated antitumor responses within the TME.

Cancer immunotherapy aims for the creation of a new immunological balance, along with impairment of tumor cells. Based on the findings in this study, multiple strategies for cancer immunotherapy are potentially effective for treatment of RCDII. First, we can explore the potential to enhance efficacy of CD8 T cells by the use of monalizumab,[27] an NKG2A-blocking agent. When combined with PD-1 blockade, this therapy not only reinvigorates CD8 T cells, but also synergistically heightens therapeutic efficacy.[22,28] Additionally, CD27 agonism could be harnessed to promote differentiation and memory formation of CD8 T cells.[29] Targeting CD4 Tregs in the RCDII TME may enhance antitumor responses, such as anticytotoxic T lymphocyte antigen 4 therapy. Lastly, targeting CD70 on tumor cells has demonstrated its potential in clinical settings.[30]

To our best knowledge, this is the first study which covers the identification and potential role of CD8 and CD4

T cells in RCDII. Herewith, it contributes to knowledge on putative antitumor and protumor responses in RCDII. This fundamental knowledge on the TME in RCDII is of crucial importance for development and evaluation of therapeutic strategies.

Supplementary Materials

Material associated with this article can be found in the online version at https://doi.org/10.1016/j.gastha.2024.08.023.

References

1. Edgar R, Domrachev M, Lash AE. Gene expression omnibus: NCBI gene expression and hybridization array data repository. Nucleic Acids Res 2002; 30(1):207–210.
2. Tack GJ, Verbeek WH, Al-Toma A, et al. Evaluation of Cladribine treatment in refractory celiac disease type II. World J Gastroenterol 2011;17(4):506–513.
3. Mukewar SS, Sharma A, Rubio-Tapia A, et al. Open-capsule budesonide for refractory celiac disease. Am J Gastroenterol 2017;112(6):959–967.
4. Schmitz F, Tjon JML, Lai Y, et al. Identification of a potential physiological precursor of aberrant cells in refractory coeliac disease type II. Gut 2013; 62(4):509.
5. Ettersperger J, Montcuquet N, Malamut G, et al. Interleukin-15-Dependent T-cell-like innate intraepithelial lymphocytes develop in the intestine and transform into lymphomas in celiac disease. Immunity 2016; 45(3):610–625.
6. Cording S, Lhermitte L, Malamut G, et al. Oncogenetic landscape of lymphomagenesis in coeliac disease. Gut 2022;71(3):497–508.
7. Soderquist CR, Lewis SK, Gru AA, et al. Immunophenotypic spectrum and genomic landscape of refractory celiac disease type II. Am J Surg Pathol 2021; 45(7):905–916.
8. Tack GJ, van Wanrooij RLJ, Langerak AW, et al. Origin and immunophenotype of aberrant IEL in RCDII patients. Mol Immunol 2012;50(4):262–270.
9. Dieckman T, Schreurs M, Mahfouz A, et al. Single-cell analysis of Refractory Celiac Disease demonstrates inter- and intra-patient aberrant cell heterogeneity. Cell Molecular Gastroenterol Hepatol 2022;14(1): 173–192.
10. Pienta KJ, McGregor N, Axelrod R, et al. Ecological therapy for cancer: defining tumors using an ecosystem paradigm suggests new opportunities for novel cancer treatments. Translational oncology 2008; 1(4):158–164.
11. Leach DR, Krummel MF, Allison JP. Enhancement of antitumor immunity by CTLA-4 blockade. Science 1996; 271(5256):1734–1736.
12. Dong Y, Sun Q, Zhang X. PD-1 and its ligands are important immune checkpoints in cancer. Oncotarget 2016;8(2):2171–2186.
13. Höllt T, Pezzotti N, van Unen V, et al. Cytosplore: interactive immune cell phenotyping for Large single-cell datasets. Comput Graph Forum 2016;35(3):171–180.
14. van Unen V, Hollt T, Pezzotti N, et al. Visual analysis of mass cytometry data by hierarchical stochastic neighbour embedding reveals rare cell types. Nat Commun 2017;8(1):1740.
15. Butler A, Hoffman P, Smibert P, et al. Integrating single-cell transcriptomic data across different conditions, technologies, and species. Nat Biotechnol 2018; 36(5):411–420.
16. Subramanian A, Tamayo P, Mootha VK, et al. Gene set enrichment analysis: a knowledge-based approach for interpreting genome-wide expression profiles. Proc Natl Acad Sci U S A 2005;102(43):15545–15550.
17. Liberzon A, Birger C, Thorvaldsdóttir H, et al. The molecular signatures database hallmark gene set collection. Cell Systems 2015;1(6):417–425.
18. Joller N, Lozano E, Burkett PR, et al. Treg cells expressing the coinhibitory molecule TIGIT selectively inhibit proinflammatory Th1 and Th17 cell responses. Immunity 2014;40(4):569–581.
19. Shevach EM, Stephens GL. The GITR–GITRL interaction: co-stimulation or contrasuppression of regulatory activity? Nat Rev Immunol 2006;6(8):613–618.
20. Collier JL, Weiss SA, Pauken KE, et al. Not-so-opposite ends of the spectrum: CD8(+) T cell dysfunction across chronic infection, cancer and autoimmunity. Nat Immunol 2021;22(7):809–819.
21. Borst L, Sluijter M, Sturm G, et al. NKG2A is a late immune checkpoint on CD8 T cells and marks repeated stimulation and cell division. Int J Cancer 2022; 150(4):688–704.
22. André P, Denis C, Soulas C, et al. Anti-NKG2A mAb is a checkpoint inhibitor that promotes anti-tumor immunity by unleashing both T and NK cells. Cell 2018; 175(7):1731–1743.e13.
23. Flieswasser T, Camara-Clayette V, Danu A, et al. Screening a broad range of solid and haematological tumour types for CD70 expression using a uniform IHC methodology as potential patient stratification method. Cancers (Basel) 2019;11(10):1611.
24. van de Ven K, Borst J. Targeting the T-cell co-stimulatory CD27/CD70 pathway in cancer immunotherapy: rationale and potential. Immunotherapy 2015;7(6):655–667.
25. Lens SMA, Drillenburg P, Den Drijver BFA, et al. Aberrant expression and reverse signalling of CD70 on malignant B cells. Br J Haematol 1999;106(2):491–503.
26. van Leeuwen MA, du Pré MF, van Wanrooij RL, et al. Changes in natural Foxp3+Treg but not mucosally-imprinted CD62LnegCD38+Foxp3+Treg in the circulation of celiac disease patients. PLoS One 2013;8(7):e68432.
27. van Hall T, André P, Horowitz A, et al. Monalizumab: inhibiting the novel immune checkpoint NKG2A. J Immunother Cancer 2019;7(1):263.
28. Busselaar J, Tian S, van Eenennaam H, et al. Helpless priming Sends CD8(+) T cells on the road to exhaustion. Front Immunol 2020;11:592569.
29. Starzer AM, Berghoff AS. New emerging targets in cancer immunotherapy: CD27 (TNFRSF7). ESMO open 2020;4(Suppl 3):e000629.

30. Flieswasser T, Van den Eynde A, Van Audenaerde J, et al. The CD70-CD27 axis in oncology: the new kids on the block. J Exp Clin Cancer Res 2022;41(1):12.

Received July 31, 2024. Accepted August 30, 2024.

Correspondence:
Address correspondence to: Frits Koning, PhD, Department of Immunology, Leiden University Medical Center, Building 1, Albinusdreef 2, 2223 ZA, Leiden, the Netherlands. e-mail: f.koning@lumc.nl.

Acknowledgments:
We thank all patients for participating in this study. We thank all gastroenterologists and endoscopy nurses for performing endoscopies and obtainment of patient samples. We thank KEA Lundin for flying to Amsterdam to provide patient samples. We thank the Leiden Genome Technology Center for their help with single-cell RNA sequencing. We thank the Flow cytometry Core Facility (FCF), LUMC for their help with flow-sorting experiments.

Authors' Contributions:
Tessa Dieckman: Conceived the study and wrote the manuscript, facilitated the obtainment of intestinal biopsies, performed mass cytometry and scRNA-seq experiments, performed flow cytometry experiments; performed data analysis for scRNA-seq data and of specific flow cytometric stainings. Mette Schreurs: Performed IF staining experiments, performed data analysis of IF stainings. Ciska Lindelauf: Performed flow cytometry experiments, performed data analysis of specific flow cytometric stainings. Ahmed Mahfouz: Performed data analysis for scRNA-seq data. Caroline R Meijer: Facilitated the obtainment of intestinal biopsies. Louise Pigeaud: Facilitated the obtainment of intestinal biopsies. Vincent van Unen: Performed data analysis for scRNA-seq data. Gerd Bouma: Conceived the study and wrote the manuscript, facilitated the obtainment of intestinal biopsies. Frits Koning: Conceived the study and wrote the manuscript.

Conflicts of interest:
The authors disclose no conflicts.

Funding:
This research was supported by the Dutch Cancer Society (KWF, grant: UL 2015-2850) and by the collaboration project TIMID (LSHM18057-SGF), financed by the public-private partnership (PPP) allowance made available by Top Sector Life Sciences & Health to Samenwerkende Gezondheidsfonden (SGF), to stimulate public-private partnerships and cofinancing by health foundations that are part of the SGF. None of the funding sources had a role in study design, collection, analysis, or interpretation of data.

Ethical Statement:
Study approved by the Medical Ethical Committee (MEC) from Amsterdam UMC, location VU Medical Center (adult samples, protocol 2017.077) and by the MEC from Leiden University Medical Center (paediatric samples, protocol 14.041). This study was performed in accordance with the local ethic guidelines and in accordance with the ethical principles from the Declaration of Helsinki.

Data Transparency Statement:
Single-cell mass cytometry data are available via FlowRepository, identifier FR-FCM-Z4X8 and FR-FCM-Z7VM. Single-cell RNA-seq data are available via NCBI's Gene Expression Omnibus (GEO),[1] accession code GSE195780. Remaining data are available from the corresponding author upon reasonable request.

Reporting Guidelines:
Declaration of Helsinki.